A Demonstration of an Improved Filtering Technique for Analyzing Climate Records via Comparisons of Satellite MSU/AMSU Instrument Temperature Products from Three Research Groups

Author: Richard E. Swanson

Poster session A21A-2137
Tuesday, 12 December 2017; 08:00 - 12:20
AGU Fall Meeting
New Orleans, LA

Abstract:

Climate data records typically exhibit considerable variation over short time scales both from natural variability and from instrumentation issues. The use of linear least squares regression can provide overall trend information from noisy data, however assessing intermediate time periods can also provide useful information unavailable from basic trend calculations. Extracting the short term information in these data for assessing changes to climate or for comparison of data series from different sources requires the application of filters to separate short period variations from longer period trends. A common method used to smooth data is the moving average, which is a simple digital filter that can distort the resulting series due to the aliasing of the sampling period into the output series. We utilized Hamming filters to compare MSU/AMSU satellite time series developed by three research groups (UAH, RSS and NOAA STAR), the results published in January 2017 (Swanson 2017).

Since the last release date for the data analyzed in that paper (July 2016), some of these groups have updated their analytical procedures and additional months of data are available to extend the series. An updated analysis of these data using the latest data releases available from each group is to be presented. Improved graphics will be employed to provide a clearer visualization of the differences between each group's results. As in the previous paper, the greatest difference between the UAH TMT series and those from the RSS and NOAA data appears during the early period of data from the MSU instruments before about 2003, as shown in the attached figures. Also presented are other findings regarding seasonal changes in the annual cycle which may be the result of either temperature changes, such as the general warming reported or the well known decline in sea-ice area in recent decades.

Background:

Filtering of time series data is a common technique for extracting information from data with noise or other variation. The simplest type of filter is a moving average, in which equal weights are applied to elements of the data, which are then summed. A moving average has a large disadvantage in that the moving average aliases the averaging period into the resulting time series, with the potential for false results. Utilizing a Hamming Filter (a modified cosine filter) reduces the distortion in the filtered time series and presents the opportunity to construct a band

pass filter by combining two filters with different averaging periods. Figure 1 shows a plot of the weights for the Hamming 7 month (H7) and Hamming 25 month (H25) filters. Also included are the weights which result from subtracting the H7 weights from the H25 weights, which, when applied to the initial series, produces a band passed series identical to that calculated by subtracting the H7 filtered series from the H25 series. The combined H7 - H25 weights are similar to those of a "Mexican Hat" filter, which is a "wavelet transform" often utilized in electrical engineering.

Figure 2 presents examples of these filtering steps using the RSS TLS North Polar data for January 1979 thru November 2017. These data were first normalized by subtracting the series average, which is necessary to remove any bias due to the selection of the base period for calculating these anomalies, as discussed in Swanson (2017). Figure 2.a presents the raw TLS data, which exhibits considerable variation on monthly time scales, variation which might be termed "noise". Figure 2.b presents the H7 result, showing the effects of the suppression of much of the short period variation, which is apparent in the reduced range of the series. Figure 2.c is the results of the H25 filter, showing even greater suppression of the variation in the series. The calculated trend is also plotted. Figure 2.d is the result of the subtraction of the H25 series from the H7 series, giving a band passed result. The trend in the H25 series of Figure 2.c (-0.12 K/decade) is almost identical to that calculated using the raw data (-0.13K/decade), while the band passed data of Figure 2.d exhibits almost no trend.

Figure 2.d highlights an exceptional cold excursion which appeared in the Spring of 1997 and which was the initial reason for this analytical effort. A question arose about the possible association with the large El Nino event of 1998 and the more recent El Nino of 2016. Since the band pass filtering trims 12 months from each end the filtered series, it was not possible to visualize the 2016 period until now, which revealed no similar excursions over the period. Other research has indicated a link between the 1997 cold event and stratospheric ozone depletion, suggesting that unusual cold conditions triggered ozone loss which then added to the cooling (Knudsen et al. 1998), (Chipperfield et al. 1999), (AMS 2017). There have been other cold excursions seen in these data, such as that of 2011, but none displaying the strength and duration of the 1997 event (Isaksen et al. 2012).

Figures 3 thru 6 are revised versions of the figures presented in (Swanson 2017), updated using the latest November 2017 releases. The difference between these plots and the earlier versions is that the revised versions use data which has been normalized, whereas in the previous versions the data had been processed by removing the trend in each series. Both processes remove the biases between the time series which result from each group's choice of base period when calculating these anomalies. As previously shown in Figure 2.d of Swanson (2017), the choice of base period can produce considerable variation in the annual data extracted using the band passed H7 minus H25 filter. UAH calculates their anomalies using a base period of 1981 thru 2010, whereas RSS uses a base period of 1979 thru 1998. For the NOAA STAR results in Figures 3-6, now present anomaly data calculated with a base period of 1980 thru 1998 for TLS and 1980 thru 1997 for TMT.

As noted in Swanson (2017), the TLS data in Figures 3.a and 3.b again display what appears to be a shift or bias difference between the UAH series and those from RSS and NOAA STAR.

This shift is also clearly seen in figures 4.a and 4.b at about 1985. The latest version of NOAA STAR TLS v4.0 shows a small shift compared with the RSS data, similar to that found in Swanson (2017).

The TMT data in Figures 5.a - 5.c are similar to those in Swanson (2017), but Figures 6.a - 6.c display the prominent differences between UAH and both RSS and NOAA STAR during the period before about 2004, during which time, the UAH data exhibits a cooling trend. One can see that that the three groups have similar trends after 2004, as the difference is nearly constant after 2004. The latest UAH TMT v6 calculation is fundamentally different from the earlier TMT v5.6, which is likely to be the cause of this difference. Not only that, but the early period with MSU data is calculated differently than the later AMSU data .

Another comparison of interest not reported previously is that between UAH v6 and the earlier UAH v5.6, using the August 2017 release date for TMT v5.6. Figures 5.d and 6.d show the respective plots for the UAH TMT v5.6 vs V6. The cross plot in 5.d shows a loop in the lower left quadrant, which indicates a short period spike in the V5.6 data, that can be seen in Figure 6.d as a downward excursion in about 1985. The cause of this spike has been discussed by several other researchers, as referenced in Swanson (2017). The difference plot in Figure 6.d also exhibits a cooling trend in the TMT v6 as compared with TMT v5.6, until about 2004 which is similar to the other early cooling trends seen in Figures 6.a and 6.b. These comparisons show that the UAH TMT v6 is warmer at the beginning than the other three series, which explains the lower overall trend calculated for the new UAH v6 data.

Additional Findings:

In recent years, satellite microwave measurements and analysis have indicated a pronounced decline in both the area and the extent of coverage. The decline in the computed area has been greatest, with projections for a continued loss of coverage at the seasonal minimum, typically occurs during September. One characteristic of the sea-ice melt season is the formation of melt ponds on the surface of the ice, especially on the young ice, which is relatively flat. As the melt season progresses, these ponds eventually tend to drain as melting breaks thru to the ocean below. The satellite passive microwave instruments and the algorithms which are used to analyze the sea-ice rely on the difference in surface emissivity between open water and sea-ice to calculate an area average for each pixel measured. The surface of the melt ponds exhibit emissivity which appears to be that of open water, thus any area of melt ponds tends to reduce the calculated ratio of ice to water for each pixel, even though there will be sea-ice remaining below the surface of the ponds. As a result, the calculated area for Arctic sea-ice will overstate the loss in sea-ice in recent years as the area of ponding has increased. Analytical support for this conclusion can be found in the paper by Kern et al. (2016) who point out that:

> "A satellite brightness temperature measurement of a mixed scene is therefore composed of contributions from the open water, i.e., cracks, leads, melt ponds, and from the (snow covered) sea ice. This has two main consequences for a sea-ice concentration product computed from such coarse-resolution satellite measurements. The sea-ice concentration in the presence of melt ponds is likely to be underestimated – because melt ponds are seen as open water."

The MSU/AMSU instruments represent another type of passive microwave measurements. Channel 2 of the MSU and 5 of the AMSU exhibit theoretical emission weighting which includes a portion of the emissions from the surface. This fact is widely acknowledged and is the reason that these data for the Troposphere are often presented as either land or ocean series, since these channels present different results over these areas. However, the Arctic Ocean represents a mix, as the high sea-ice emissivity and lower emissivity of water will appear be combined into the measurements at each scan position throughout the seasonal cycle. See Groody et al. (2004), Appendix A. If the sea-ice annual cycle were relatively constant over the years of measurement data, this would not be a large problem, however, as the area of melt ponds appears to be increasing, the change in the seasonal measurements would impact the MSU/AMSU data as a cooling trend.

The filtering techniques from Swanson (2017) were applied to analyze the RSS TLT for the Arctic, band pass filtering both the land and ocean time series, which allowed the visualization of the remnant annual cycle which resides in those time series, as described above. The band passed series were split in half, with an April thru September portion defined as Melt season and an October thru March portion as Freeze season. Figure 7.a presents the results for the combined land and ocean data and Figure 7.b is for ocean only. The RSS results showed a pronounced cooling trend in the ocean data for the Melt season and a warming trend for the Freeze season.

Monthly trends for the RSS TLT and TMT and NOAA TMT band passed series were calculated in order to compare land and ocean groupings, shown in Figures 8.a thru 8.d. For the high latitude ocean data, the months of June and July exhibited the strongest cooling, while December and January showed the strongest warming. The land only data showed a different seasonal result than that of the high latitude ocean, with weak warming during the Summer months and slight cooling during Winter. The fact that the Summer months produce cooling over the high latitude oceans strongly points to the sea-ice melting as a cause, given that it's well known that the Summer sea-ice has evidenced a steady decline, especially since the turn of the century.

Conclusions:

The evidence presented in this study appear to indicate that the Arctic annual sea-ice cycle may be impacting the MSU/AMSU satellite brightness temperature data which has been used to assess Arctic climate change. Given the numerous reports of Arctic warming over land, the continuing loss of Arctic sea-ice extent and the replacement of older multi year ice with first year ice, it seems highly unlikely that the high latitude cooling over the ocean, as found by this analysis, represents the actual situation. These results support the hypothesis that trends in the satellite data for the Lower Troposphere over the Arctic Ocean include an a negative trend due to changes in the annual sea-ice cycle. There are several additional complicating factors to be considered in assessing this hypothesis, such as the effect of binning the data into a 2.5×2.5 degree grid, which would tend to include areas with both land and ocean in many grid boxes, as well as the fact that the high latitude areas designated as oceans include regions which have not experienced sea-ice during the recent past. Further comparisons with other sources of temperature data, such as balloon data (Swanson 2003), would be helpful in determining whether the satellite data represents the actual atmospheric temperature trends in the Arctic Troposphere.

References:

AMS (2017), State of the Climate in 2016, Chap 5, section J., BAMS 2017.
http://www.ametsoc.net/sotc2016/Ch05_Arctic.pdf

Chipperfield, M. P., and R. L. Jones (1999), Relative influences of atmospheric chemistry and transport on Arctic ozone trends, Nature, 400(6744), 551–554.
http://dx.doi.org/10.1038/22999

Grody, N. C., K. Y. Vinnikov, M. D. Goldberg, J. T. Sullivan, and J. D. Tarpley (2004), Calibration of multisatellite observations for climatic studies: Microwave Sounding Unit (MSU), *J. Geophys. Res.*, **109**, D24104.
https://doi.org/10.1029/2004JD005079

Isaksen, I. S. A., Zerefos, C., Wang, W.-C., Balis, D., Eleftheratos, K., Rognerud, B., Stordal, F., Berntsen, T. K., LaCasce, J. H., Søvde, O. A, Olivié, D., Orsolini, Y. J., Zyrichidou, I., Prather, M., and Tuinder, O. N. E., (2012), Attribution of the Arctic ozone column deficit in March 2011, *Geophys Res Let.* **39**,
http://dx.doi.org/10.1029/2012GL053876

Kern, S., Rösel, A., Pedersen, L. T., Ivanova, N., Saldo, R., and Tonboe, R. T. (2016): The impact of melt ponds on summertime microwave brightness temperatures and sea-ice concentrations, The Cryosphere, 10, 2217-2239, https://doi.org/10.5194/tc-10-2217-2016.
https://www.the-cryosphere.net/10/2217/2016/

Knudsen, B. M., N. Larsen, I. S. Mikkelsen, J. J. Morcrette, G. O. Braathen, E. Kyrö, H. Fast, H. Gernandt, H. Kanzawa, H. Nakane, V. Dorokhov, V. Yushkov, G. Hansen, M. Gil, R. J. Shearman (1998), Ozone depletion in and below the Arctic Vortex for 1997, *Geophys Res Let.* **25**, 627.
http://dx.doi.org/10.1029/98GL00300

Spencer, R. W., Christy, J. R. and Braswell1, W. D. (2016), UAH Version 6 Global Satellite Temperature Products: Methodology and Results, *Asia-Pacific J. Atmos. Sci.*

Swanson, R. E., (2003), Evidence of possible sea-ice influence on Microwave Sounding Unit tropospheric temperature trends in polar regions, *Geophys. Res. Let.* **30**, 2040.
http://dx.doi.org/10.1029/2003GL017938

Swanson (2017), A Comparative Analysis of Data Derived from Orbiting MSU/AMSU Instruments, *J. Ocean and Atmos. Tech*, Jan 2017.
http://dx.doi.org/10.1175/JTECH-D-16-0121.1

Contact: e-mail address: e_swanson@skybest.com

Figure 1

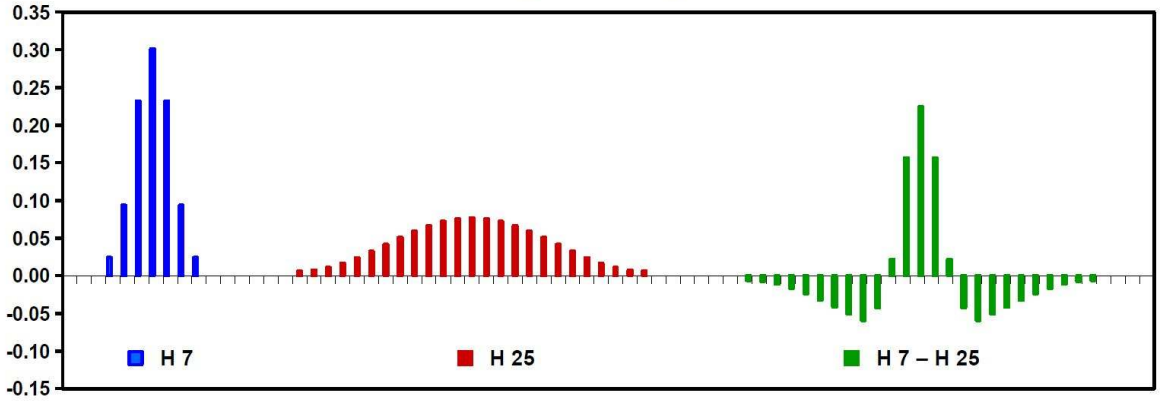
Hamming Filter Weights
0.35
0.30
0.25
0.20
0.15
0.10
0.05
0.00
-0.05
-0.10
-0.15
H 7
H 25
H 7 – H 25

2.a

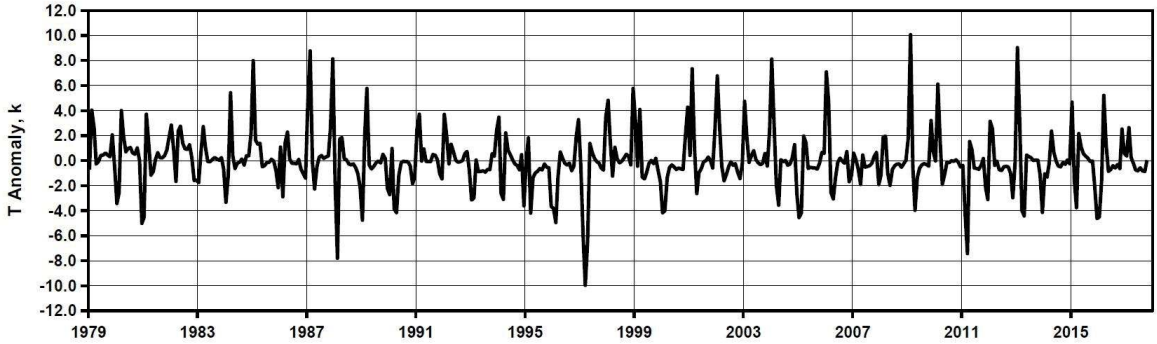
T Anomaly, k
12.0
10.0
8.0
6.0
4.0
2.0
0.0
-2.0
-4.0
-6.0
-8.0
-10.0
-12.0
1979
1983
1987
1991
1995
1999
2003
2007
2011
2015

2.b

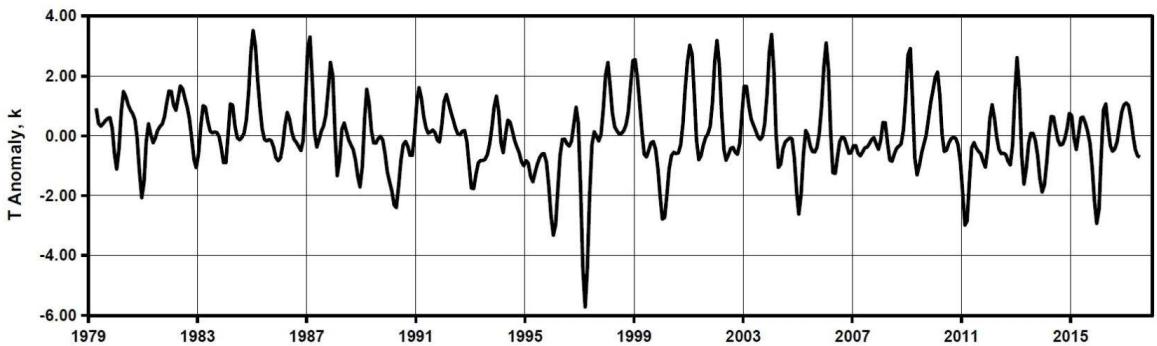
T Anomaly, k
4.00
2.00
0.00
-2.00
-4.00
-6.00
1979
1983
1987
1991
1995
1999
2003
2007
2011
2015

2.c

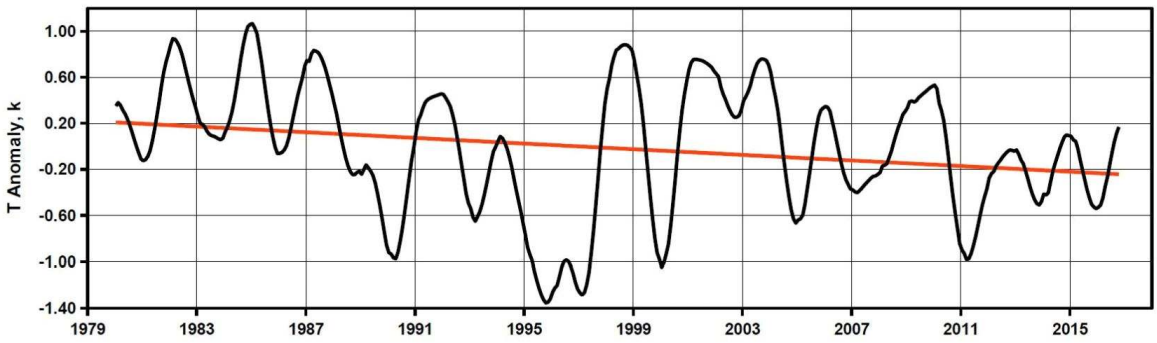
T Anomaly, k
1.00
0.60
0.20
-0.20
-0.60
-1.00
-1.40
1979
1983
1987
1991
1995
1999
2003
2007
2011
2015

2.d

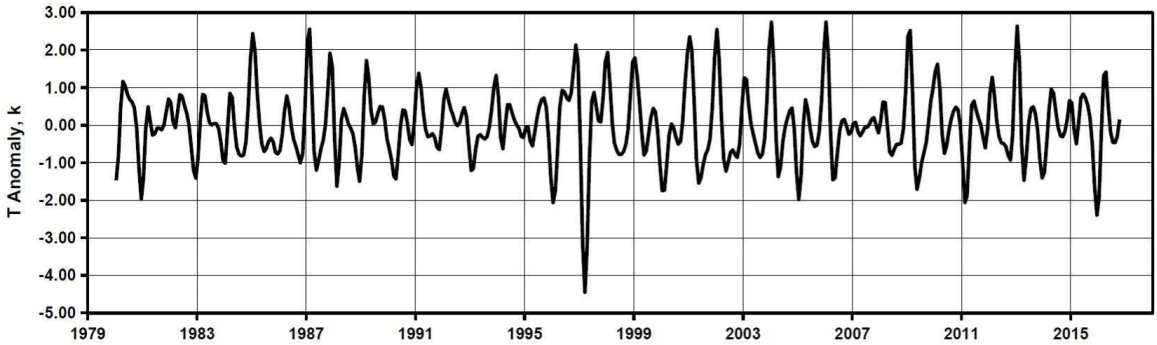
T Anomaly, k
3.00
2.00
1.00
0.00
-1.00
-2.00
-3.00
-4.00
-5.00
1979
1983
1987
1991
1995
1999
2003
2007
2011
2015

3.a revised

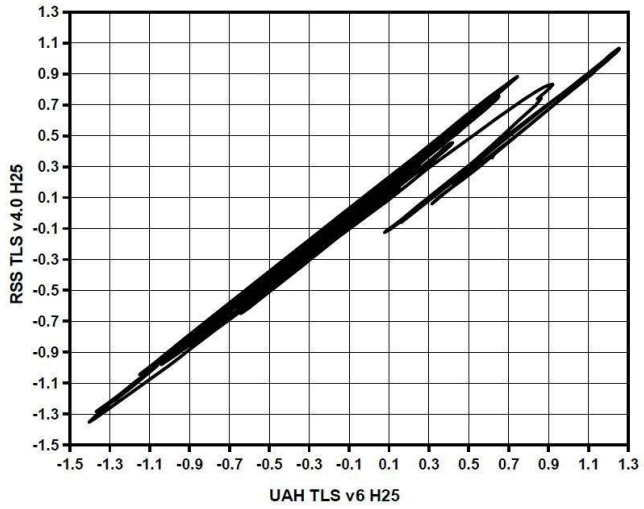

3.b revised

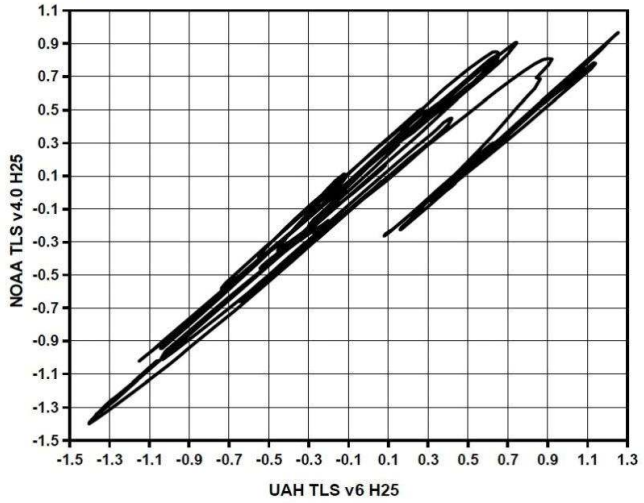

3.c revised

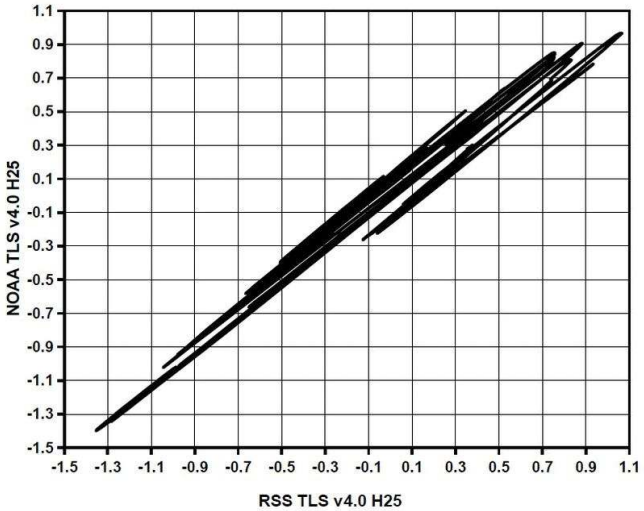

4.a revised

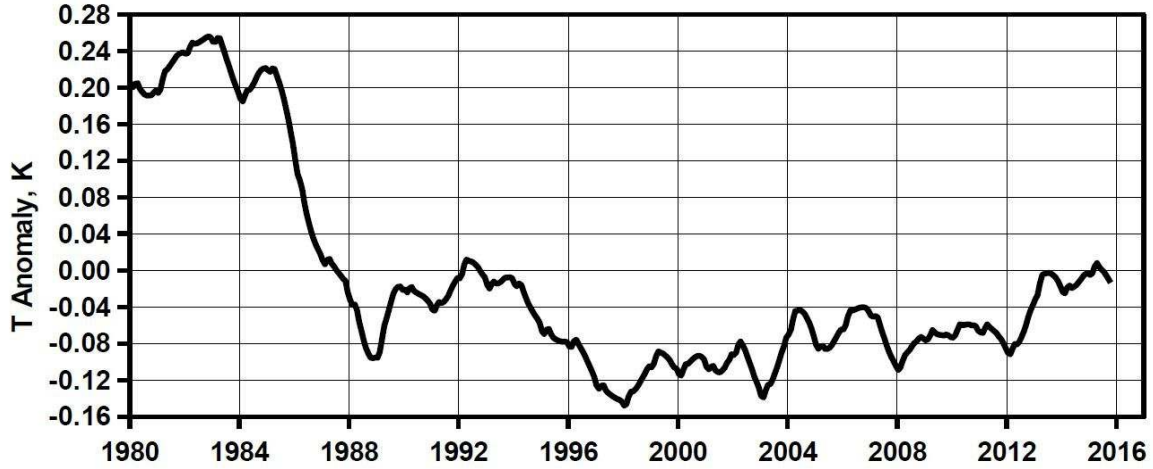

4.b revised

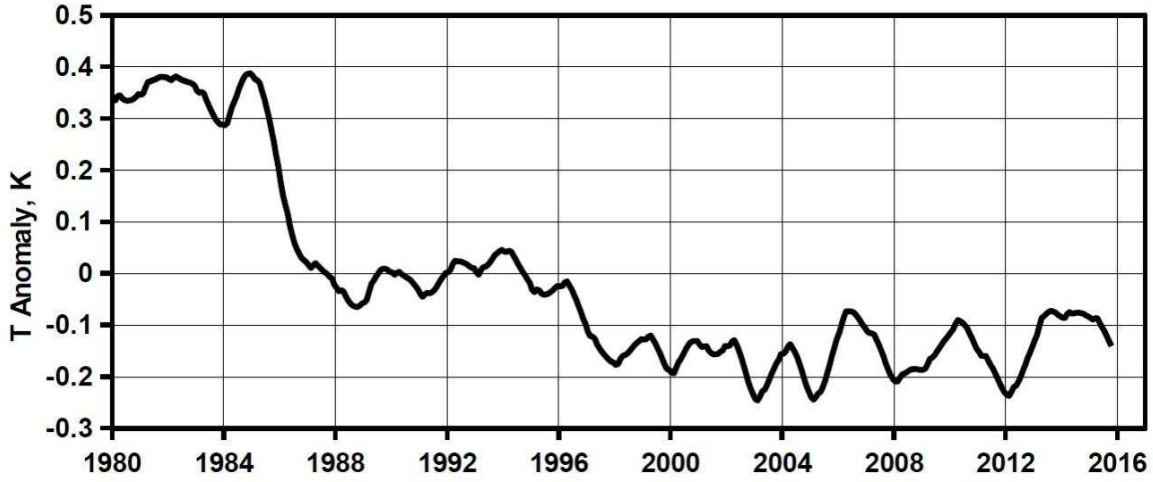

4.c revised

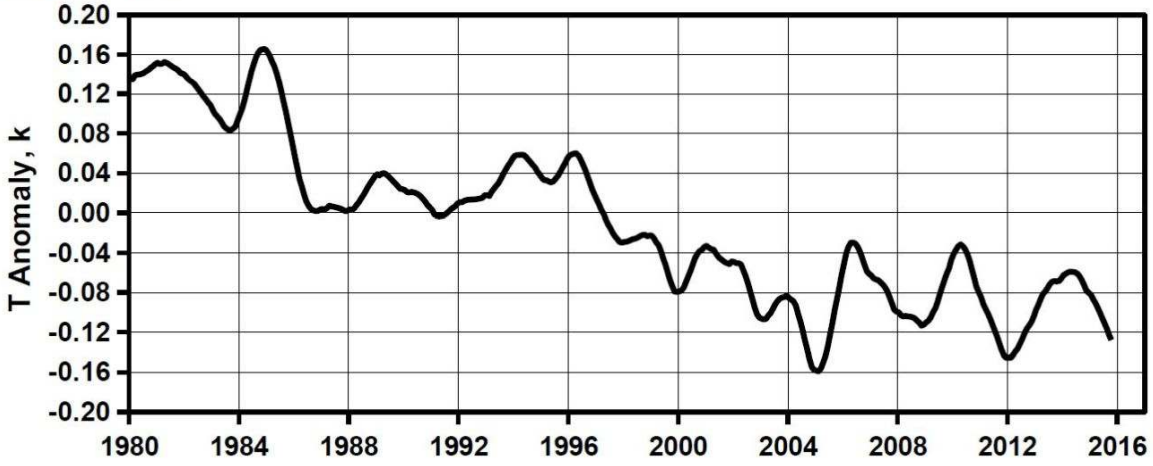

5.a revised

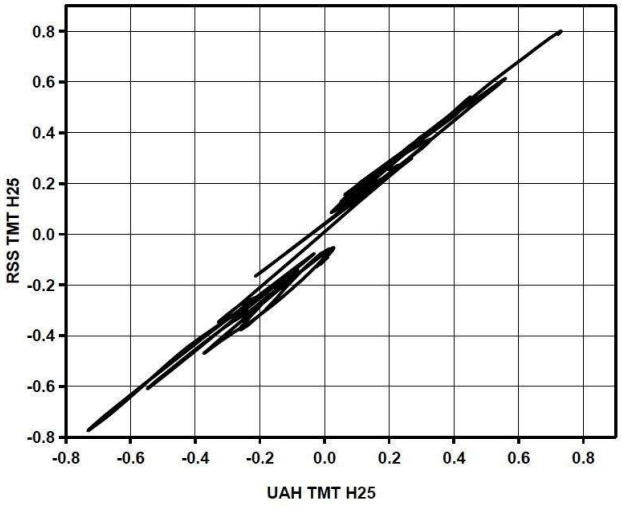

5.b revised

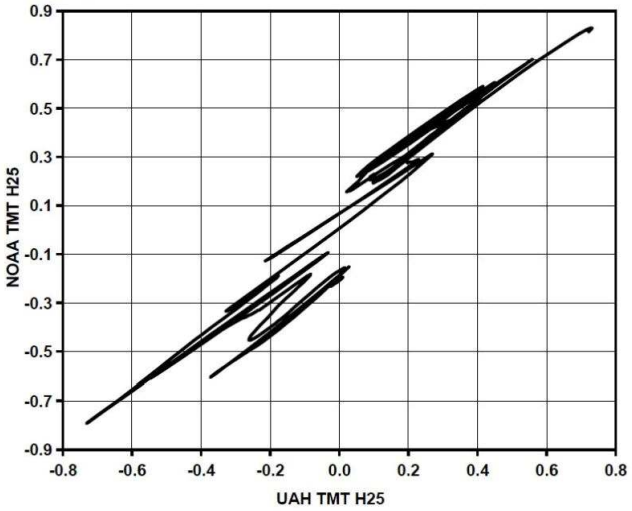

5.c revised

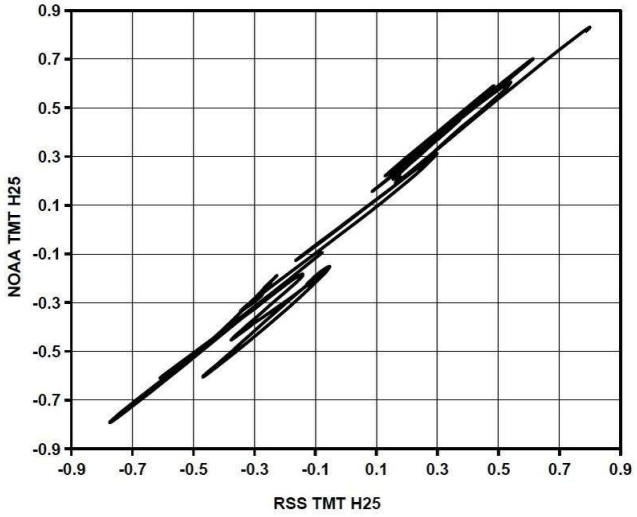

5.d

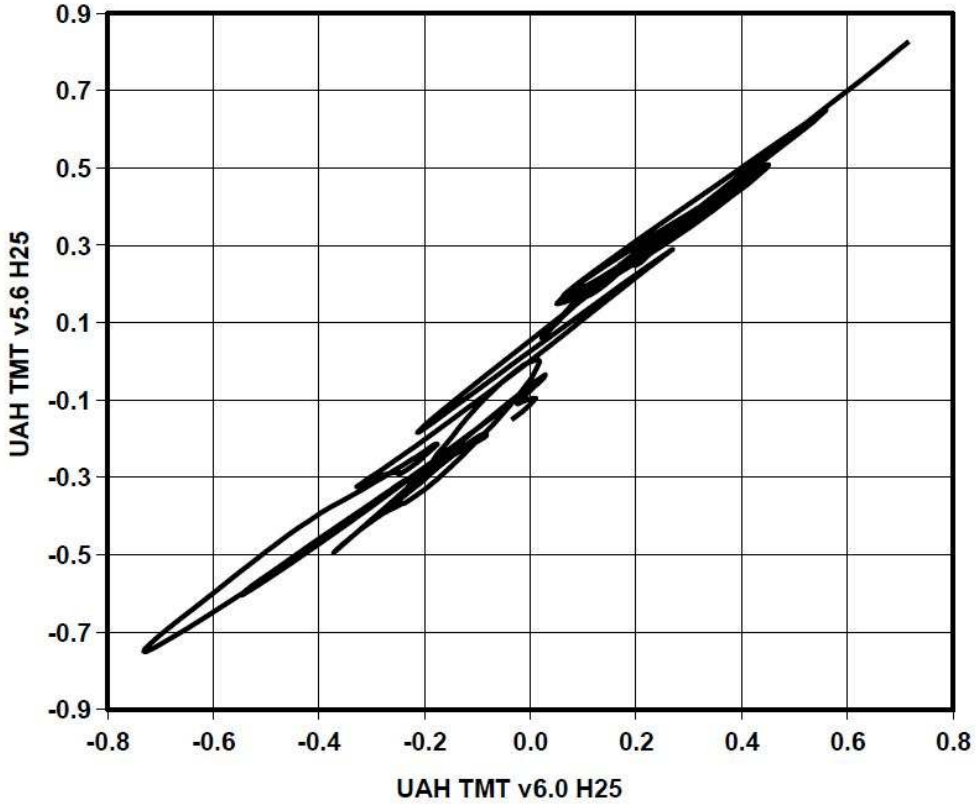
0.9
0.7
0.5
0.3
0.1
-0.1
-0.3
-0.5
-0.7
-0.9
UAH TMT v5.6 H25
-0.8
-0.6
-0.4
-0.2
0.0
0.2
0.4
0.6
0.8
UAH TMT v6.0 H25

6.d

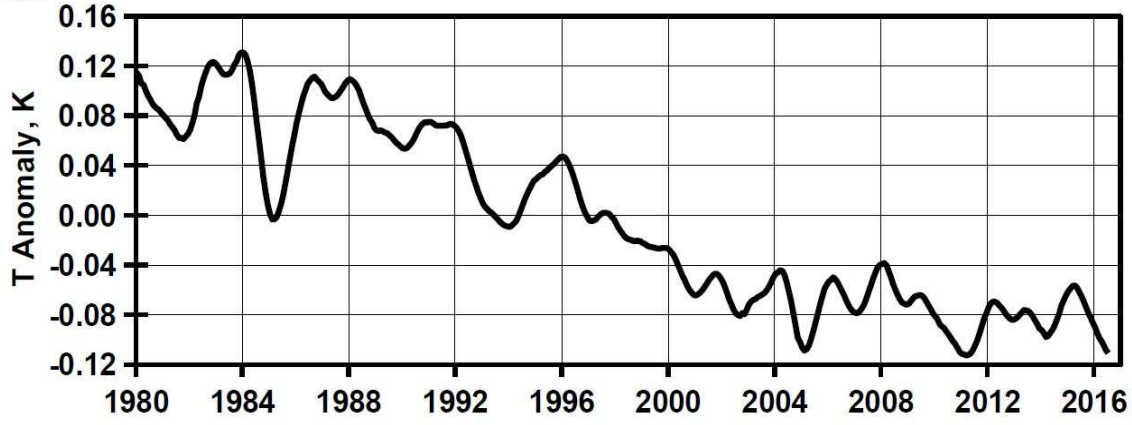
0.16
0.12
0.08
0.04
0.00
-0.04
-0.08
-0.12
T Anomaly, K
1980
1984
1988
1992
1996
2000
2004
2008
2012
2016

6.a revised

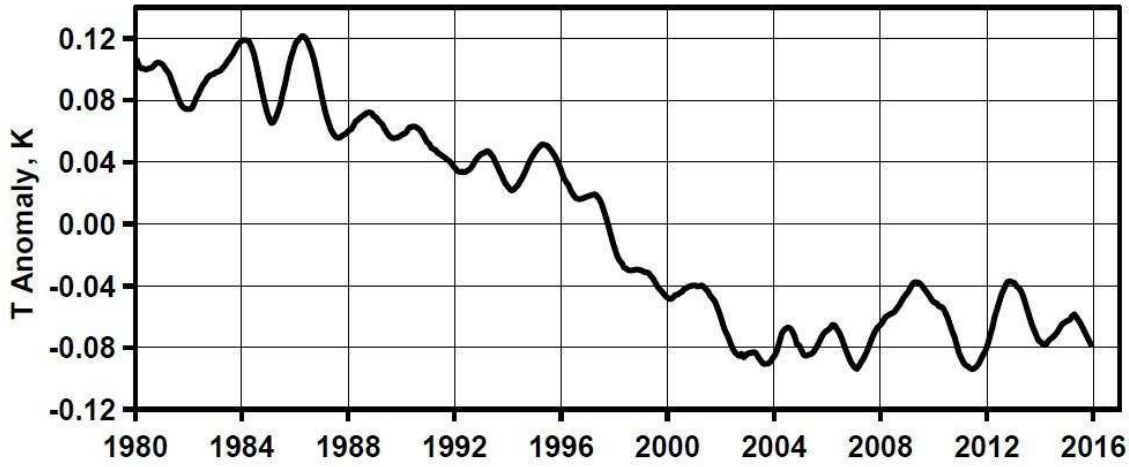

6.b revised

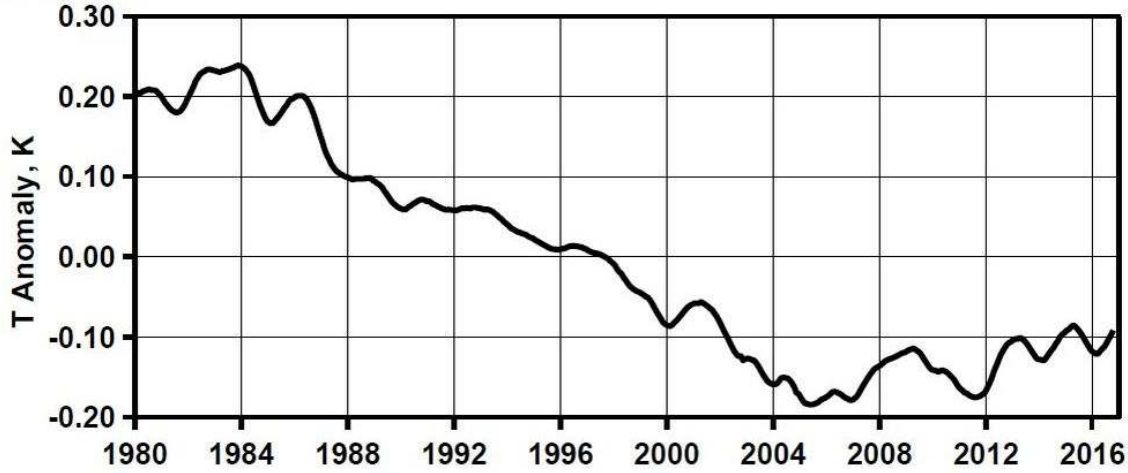

6.c revised

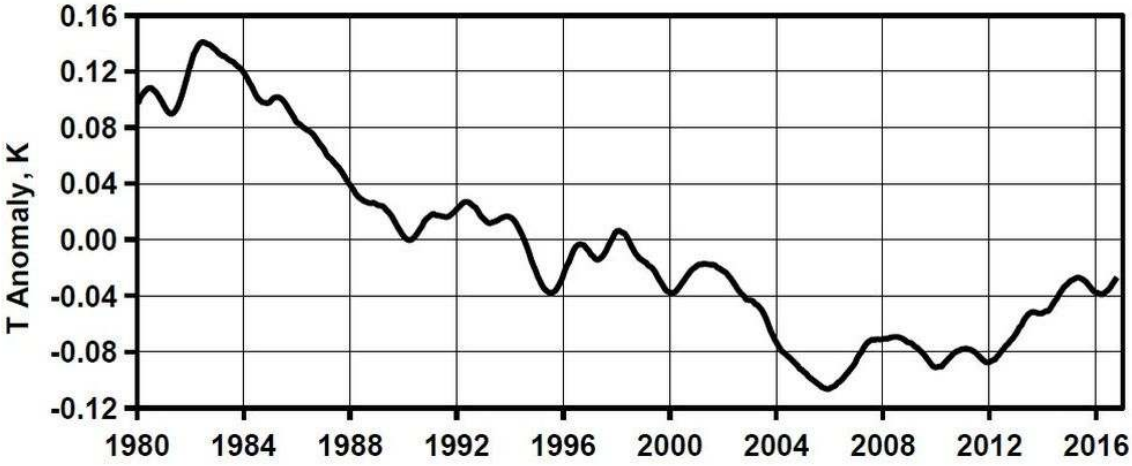

7.a

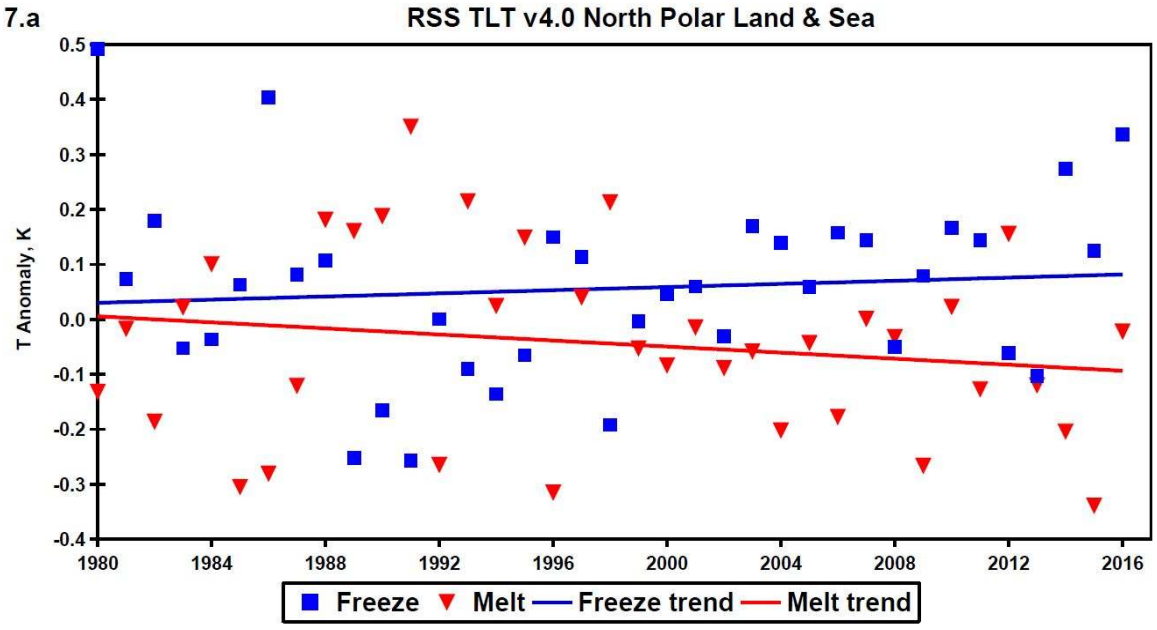
RSS TLT v4.0 North Polar Land & Sea
T Anomaly, K
0.5
0.4
0.3
0.2
0.1
0.0
-0.1
-0.2
-0.3
-0.4
1980
1984
1988
1992
1996
2000
2004
2008
2012
2016
Freeze
Melt
Freeze trend
Melt trend

7.b

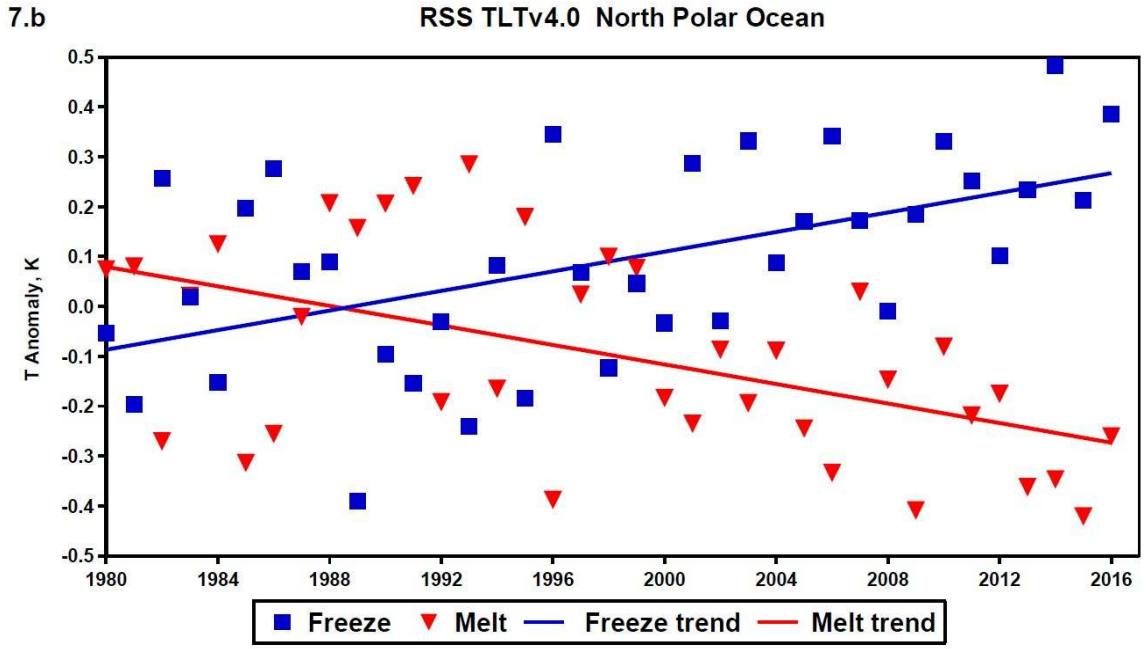
RSS TLTv4.0 North Polar Ocean
T Anomaly, K
0.5
0.4
0.3
0.2
0.1
0.0
-0.1
-0.2
-0.3
-0.4
-0.5
1980
1984
1988
1992
1996
2000
2004
2008
2012
2016
Freeze
Melt
Freeze trend
Melt trend

8.a

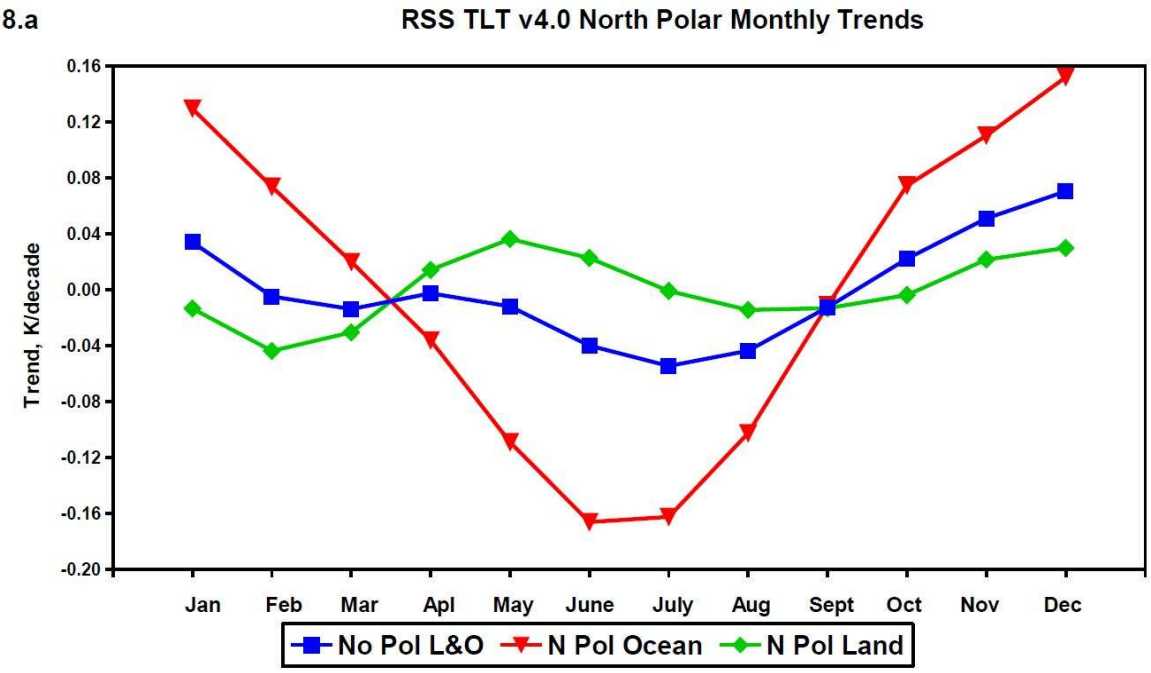
RSS TLT v4.0 North Polar Monthly Trends
Trend, K/decade
0.16
0.12
0.08
0.04
0.00
-0.04
-0.08
-0.12
-0.16
-0.20
Jan
Feb
Mar
Apl
May
June
July
Aug
Sept
Oct
Nov
Dec
No Pol L&O
N Pol Ocean
N Pol Land

8.b

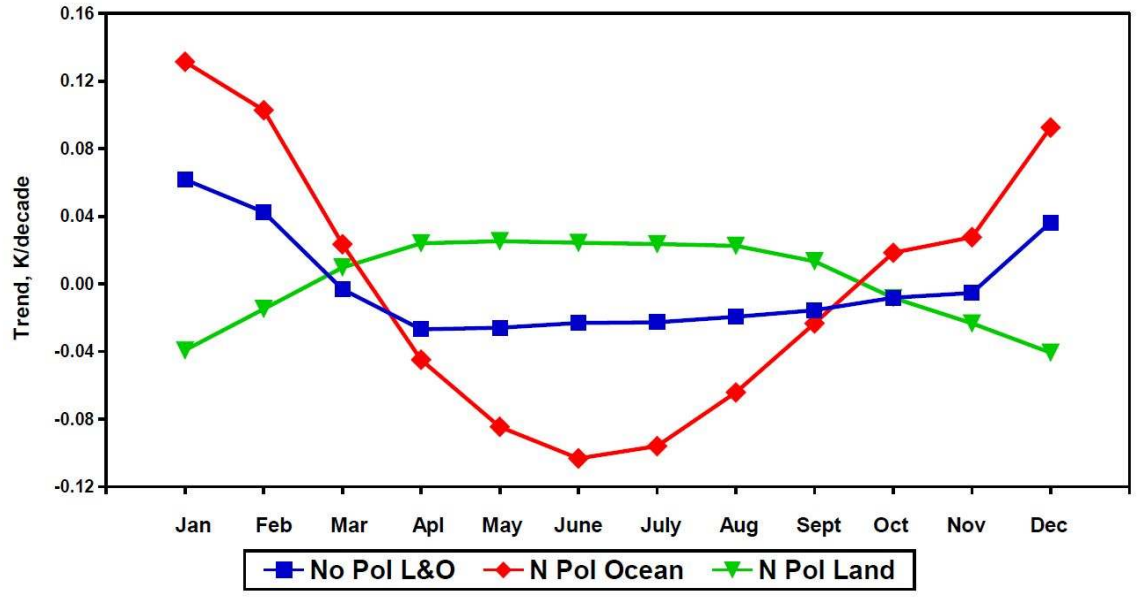
RSS TMT v4.0 North Polar Monthly Trends
Trend, K/decade
0.16
0.12
0.08
0.04
0.00
-0.04
-0.08
-0.12
Jan
Feb
Mar
Apl
May
June
July
Aug
Sept
Oct
Nov
Dec
No Pol L&O
N Pol Ocean
N Pol Land

8.c

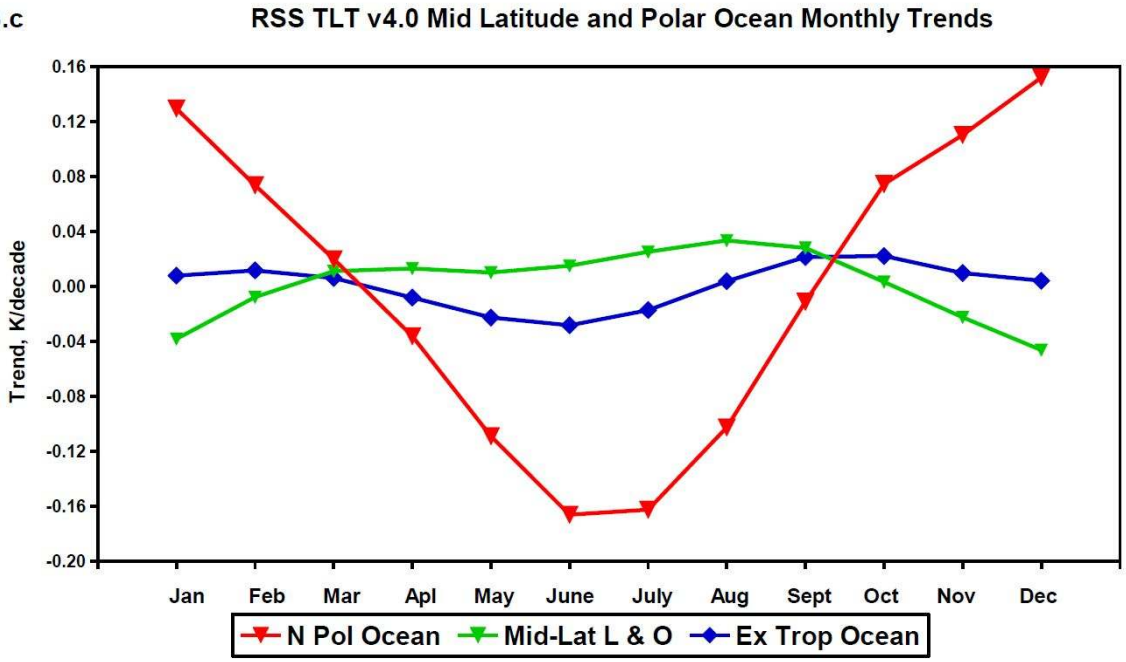
RSS TLT v4.0 Mid Latitude and Polar Ocean Monthly Trends
Trend, K/decade
0.16
0.12
0.08
0.04
0.00
-0.04
-0.08
-0.12
-0.16
-0.20
Jan
Feb
Mar
Apl
May
June
July
Aug
Sept
Oct
Nov
Dec
N Pol Ocean
Mid-Lat L & O
Ex Trop Ocean

8.d

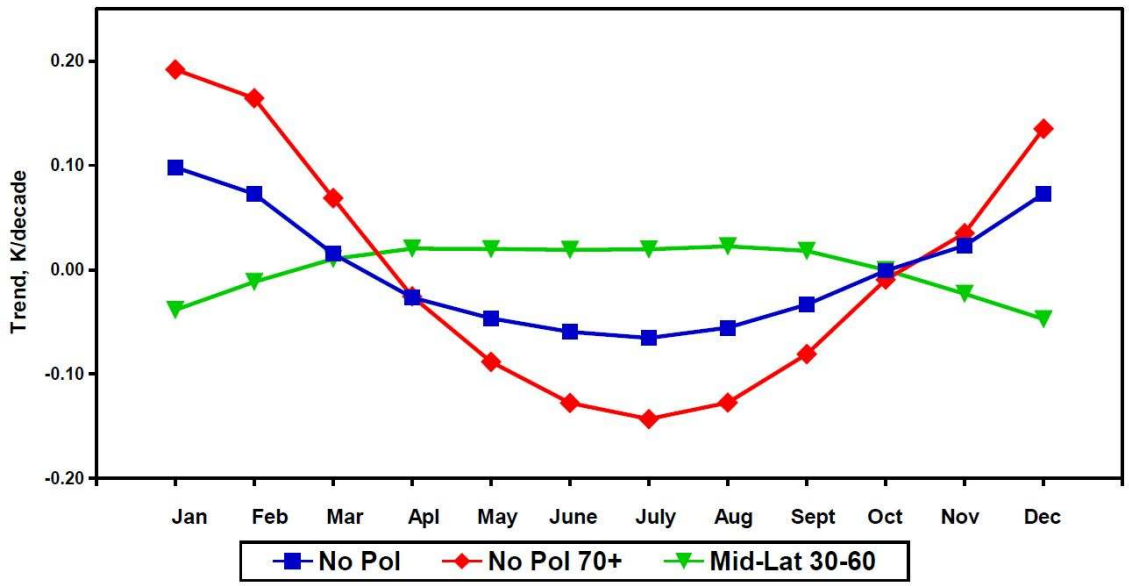
NOAA STAR TMT v4.0 Polar and Mid-lat Monthly Trends
Trend, K/decade
0.20
0.10
0.00
-0.10
-0.20
Jan
Feb
Mar
Apl
May
June
July
Aug
Sept
Oct
Nov
Dec
No Pol
No Pol 70+
Mid-Lat 30-60